aerospace

MDPI

Article

Predefined-Time Heading Control for a 9-DOF Parafoil Recovery System Subject to Internal Relative Motions

Yiming Guo *, Jianguo Yan, Xiaojun Xing, Xiwei Wu and Lingwei Li

Automation School, Northwestern Polytechnical University, Xi'an 710072, China
* Correspondence: gjm629@mail.nwpu.edu.cn; Tel.: +86-1331-918-9173

Abstract: This paper addresses the challenging problem of predefined-time heading control of a parafoil recovery system (PRS) with internal relative motions and external disturbance. On the basis of the PRS described by a 9-degree-of-freedom model, a simplification and equivalent model is first derived, which is convenient to design control law. Then, a predefined-time disturbance observer is provided to estimate the lumped disturbance caused by internal relative motions and apparent mass. With the application of the disturbance estimation, a predefined-time heading controller is developed for the PRS. The control system is proven to be predefined-time stable by Lyapunov theory. Simulation results illustrate that the proposed method has better control performance than finite-time and PID controllers.

Keywords: parafoil recovery system; predefined-time control; disturbance observer; multibody model; backstepping control

Citation: Guo , Y.; Yan, J.; Xing, X.; Wu, X.; Li, L. Predefined-Time Heading Control for a 9-DOF Parafoil Recovery System Subject to Internal Relative Motions. *Aerospace* **2023**, *10*, 348. https://doi.org/10.3390/aerospace10040348

Academic Editor: Ziquan Yu

Received: 29 December 2022
Revised: 9 March 2023
Accepted: 23 March 2023
Published: 3 April 2023

1. Introduction

In recent years, the parafoil recovery system (RPS) has attracted wide publicity [1,2]. It can be widely used in both military and civil areas for good flight stability and loading capacity [3–6]. Unlike conventional aircraft, this system consists of three subsystems, i.e., parafoil, on-board controller, and payload [7]. It leads to internal relative motion between subsystems during the flight process, which affects the PRS attitude and translation motions [8]. The PRS is also affected by the apparent mass due to the small rigid mass of the parafoil [9,10]. Although the development of heading control design for the PRS has been witnessed in the past three decades, there is not a systematic research framework combining complex models with advanced control methods. This problem is still open.

Before designing the control scheme, it is necessary to establish the mathematical model to describe the PRS. The parafoil system is regarded as a rigid body without internal relative motions in most early works. For example, a 6-degrees-of-freedom (DOF) model, neglecting minor and coupling terms, was expressed in [11]. In [12], a 6-DOF parafoil model was provided using the natural motion principle and the airdropping procedure results. To improve the fidelity of the model, Slegers, et al. developed the 7-DOF model, allowing the relative yawing motion of a payload with respect to the parafoil [13,14]. The PRS was established by an 8-DOF Kirchhoff motion equation in [15,16]. Unlike an 8-DOF parafoil, whose payload is also connected to the canopy at two points, a 9-DOF model was developed in [17]. The 9-DOF type is performed by the inclining lift of the canopy rather than by applying the brakes to generate the yaw moment as in the 8-DOF type. However, the rapid development of high-fidelity models has not promoted the progress of model-based control theory in the PRS field. One important reason is that the high-fidelity model brings more nonlinear coupling, which makes it very difficult to design control laws directly based on the model. This fact hinders the generation of advanced control schemes for the PRS.

In the existing literature on designing controllers for the PRS, there are two types of approaches. One is to develop the linear control method based on the small perturbation model [18–23]. For instance, a model predictive controller was designed based on a reduced state linear model in [18]. In [19], an adaptive $\mathcal{L}_1$ heading controller was developed for the PRS described by a linear time-invariant model. The control signals are kept stable in the face of noise and uncertain dynamics. In [20], the optimal control approach was used to generate closed-form guidance law. In [21], a PID controller was provided to deal with the heading tracking problem. This work pointed out that the linear-quadratic regulator and model predictive control were too complex for the autopilot to handle.

In the linear control design, the internal relative motions, the apparent mass disturbance, and the aerodynamic uncertainties were not rejected. In contrast, another approach, designing a nonlinear controller based on the high-fidelity model [24–26] to achieve tracking control with good accuracy, is to reject disturbances and uncertainties. In [24], the nonlinear dynamic inversion technique was used to propose a generic heading tracking controller for the 9-DOF multibody dynamics model. An active disturbance rejection controller was developed for an 8-DOF model in [27]. The total disturbance was estimated by the extended state observer, and then the controller was designed to compensate for it. Moreover, an active disturbance rejection controller with feedforward compensation was designed in [25], which can further improve the anti-interference performance. It is seen that model-free control is the mainstream method of parafoil control because its flexible multi-body structure will make the design with model control more complex. Although this control method has good generality, it is difficult to further theoretically improve the control performance.

To further achieve a fast tracking stabilization maneuver, a finite-time tracking control scheme was designed in [28] for the powered parafoil system. Although the proposed method improved the tracking rate of the inner-loop yaw angle, it does not consider the heading change. Another work is that an adaptive fixed-time tracking controller was provided for the 9-DOF PRS model in [26]. However, the existing fixed-time control schemes have a technical problem, that is, the upper bound of the settling time is a complex function of the control parameters [29]. It is difficult for designers to schedule the required convergence time in advance. Introducing the predefined-time theory into the parafoil heading control is the original motivation of this paper.

Motivated by the descriptions mentioned above, a predefined-time heading tracking controller for a PRS described by the 9-DOF model is proposed in this paper. The main contributions of this paper are highlighted as follows.

1. *Most existing works used model-free control due to the complex nonlinearity of the parafoil system. Unlike these methods, a simplification and equivalent model from a 9-DOF multibody dynamics is provided first. The proposed model can be directly used for advanced control design.*
2. *This paper may be the first result to solve the heading tracking control problem of a PRS by using the observer-based predefined-time control. Different from general observer-based control, the proposed controller can be achieved in a predefined time without any upper bound of the lumped disturbance.*
3. *With the application of disturbance estimation, a predefined-time heading tracking controller is developed. The proposed observer-based controller has better control performance than finite-time and PID controllers.*

The rest of this paper is organized as follows. Some preliminaries are given in Section 2. In Section 3, an equivalent model from a 9-DOF multibody dynamics is established. In Section 4, a predefined-time heading tracking controller is developed. The simulation results are given in Section 5, and some conclusion remarks are given in Section 6.

2. Preliminaries

Definition 1. *Consider the autonomous dynamical system*

$$\dot{\boldsymbol{x}} = \boldsymbol{f}(t, \boldsymbol{x}), \boldsymbol{f}(\mathbf{0}) = \mathbf{0}, \boldsymbol{x}(\mathbf{0}) = \boldsymbol{x}_0 \tag{1}$$

for the state $\boldsymbol{x} \in \mathbb{R}^n$. $\boldsymbol{f}(\boldsymbol{x}) : \mathbb{R}^n \to \mathbb{R}^n$ is a nonlinear and locally Lebesgue-integrable function. For the system parameters $\boldsymbol{\rho}$ and a constant $T_c = T_c(\boldsymbol{\rho}) > 0$, the origin of system (1) is viewed to be predefined time stable if it is fixed time stable and the settling-time function $T : \mathbb{R}^n \to \mathbb{R}$ is such that

$$T(\boldsymbol{x}_0) \leq T_c, \forall \boldsymbol{x}_0 \in \mathbb{R}^n \tag{2}$$

where T_c is called a predefined-time [30].

Lemma 1. *Denote an uncertain dynamic system*

$$\dot{\boldsymbol{x}} = \boldsymbol{f}(t, \boldsymbol{x}, \boldsymbol{d}) \tag{3}$$

with disturbance vector $\boldsymbol{d} \in \mathbb{R}^n$. If there exists a radially unbounded Lyapunov function $V(\boldsymbol{x}) : \mathbb{R}^n \to \mathbb{R}$ such that

$$\dot{V} \leq -\frac{\pi}{\eta T_c}\left(V^{1-\frac{\eta}{2}} + V^{1+\frac{\eta}{2}}\right) \tag{4}$$

for any solution $\boldsymbol{x}(t, \boldsymbol{x}_0)$ of system (3), where $T_c > 0$ is predefined constant and $\eta \in (0, 1)$ is gain, then the equilibrium of the system is predefined time stable, and the settling time is T_c [31].

3. Dynamic Model of a PRS and Problem Formulation

As we known, the parafoil system is generally established with a 9-DOF model, which considers the coupling between the subsystems explicitly. The model consists of three subsystems: parafoil, payload, and on-board controller. The system includes three translational motions of system's center O_c, three rotational motions of the parafoil's center O_p, and three rotational motions of the payload's center O_b. The on-board-controller is installed between the parafoil and the payload, and the actuators of the controller can be directly driven by the control command. The control ropes connect the trailing edge of the parafoil canopy and the actuators. In the control process, the length of the control ropes can be changed by the actuators, and then the trailing edges of the canopy are deflected. The asymmetric deflection of the trailing edges causes the aerodynamic characteristics of the canopy to change, which leads to a change in the heading angle. It is also the only control quantity of the PRS.

The system structure and four coordinate frames to establish the 9-DOF model of a PRS is illustrated in Figure 1. $\mathcal{F}_e X_e Y_e Z_e$ is the Earth-fixed inertial frame with the origin O_e being an arbitrary point on the ground. $\mathcal{F}_c X_c Y_c Z_c$ is another reference frame with the origin being the controller's center O_c, whose axes are parallel to that of $\mathcal{F}_e$. Both $\mathcal{F}_p X_p Y_p Z_p$ and $\mathcal{F}_b X_b Y_b Z_b$ are body-fixed frame, and their coordinate origins are parafoil's center O_p and payload's center O_b, respectively. $\boldsymbol{X}_{cp} \in \mathbb{R}^3$ and $\boldsymbol{X}_{cb} \in \mathbb{R}^3$ represents the distance between the parafoil's center O_p and the controller's center O_c, and the distance between the payload's center O_p and the controller's center O_c, respectively.

To represent the position orientation of the PRS with respect to $\mathcal{F}_e$, the inertial position $\boldsymbol{P}_e = [X_e \quad Y_e \quad Z_e]^T$ and the inertial velocity $\boldsymbol{V}_c = [u_c \quad v_c \quad w_c]^T$ are adopted. Assuming that the subscript $i = \mathrm{p}$ and $i = \mathrm{b}$ denote the parafoil and the payload, Euler angles $\boldsymbol{\Theta}_i = [\phi_i \quad \theta_i \quad \psi_i]^T$ and the angular velocities $\boldsymbol{\omega}_i = [\omega_{i1} \quad \omega_{i2} \quad \omega_{i3}]^T$ are employed to represent the attitude orientation of the subsystems. Let $\boldsymbol{V}_i \in \mathbb{R}^3$ be the linear velocities of the subsystem with respect to $\mathcal{F}_i$. With the application of the Euler conversion formula, the transform matrix of the angular velocity and the linear velocity are defined as $\boldsymbol{G}_i \in \mathbb{R}^{3\times3}$ and $\boldsymbol{T}_{i-c} \in \mathbb{R}^{3\times3}$, such as

$$\boldsymbol{G}_i = \begin{bmatrix} 1 & \sin\phi_i \tan\theta_i & \cos\phi_i \tan\theta_i \\ 0 & \cos\theta_i & -\sin\phi_i \\ 0 & \sin\phi_i/\cos\theta_i & \cos\phi_i/\cos\theta_i \end{bmatrix} \tag{5}$$

$$\boldsymbol{T}_{i-c} = \begin{bmatrix} \cos\theta_i \cos\psi_i & \cos\theta_i \sin\psi_i & -\sin\theta_i \\ \sin\phi_i \sin\theta_i \cos\psi_i - \cos\phi_i \sin\psi_i & \sin\phi_i \sin\theta_i \sin\psi_i + \cos\phi_i \cos\psi_i & \sin\phi_i \cos\theta_i \\ \cos\phi_i \sin\theta_i \cos\psi_i + \sin\phi_i \sin\psi_i & \cos\phi_i \sin\theta_i \sin\psi_i - \sin\phi_i \cos\psi_i & \cos\phi_i \cos\theta_i \end{bmatrix}. \tag{6}$$

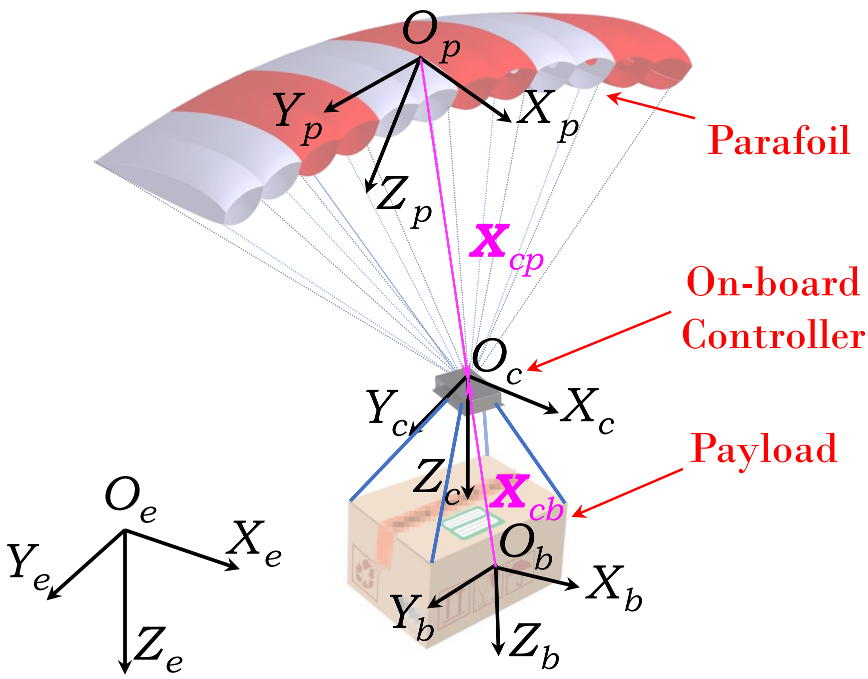

Figure 1. Structure of a PRS and its coordinate reference frames.

3.1. Dynamic Equations of the Parafoil

According to [26], the forces and moments of the parafoil are primarily because of four sources, namely, aerodynamics, gravity, apparent mass, and suspension lines. Letting $\boldsymbol{F}_{\mathrm{p}}^{\mathrm{aero}} \in \mathbb{R}^3$ and $\boldsymbol{M}_{\mathrm{p}}^{\mathrm{aero}} \in \mathbb{R}^3$ be the forces and moments due to aerodynamics, $\boldsymbol{F}^{\mathrm{app}} \in \mathbb{R}^3$ and $\boldsymbol{M}^{\mathrm{app}} \in \mathbb{R}^3$ be the forces and moments due to the apparent mass $\boldsymbol{M}_{\mathrm{f}} \in \mathbb{R}^{3\times3}$ and $\boldsymbol{I}_{\mathrm{f}} \in \mathbb{R}^{3\times3}$, and $\boldsymbol{F}_{\mathrm{r}} \in \mathbb{R}^3$ and $\boldsymbol{M}_{\mathrm{r}} \in \mathbb{R}^3$ be the forces and moments due to the suspension lines, the parafoil dynamic equations can be described as follows:

$$m_{\mathrm{p}}\dot{\boldsymbol{V}}_{\mathrm{p}} = m_{\mathrm{p}} g \boldsymbol{z}_{\mathrm{p}} + \boldsymbol{F}_{\mathrm{p}}^{\mathrm{aero}} + \boldsymbol{F}^{\mathrm{app}} - \boldsymbol{T}_{\mathrm{p-c}}\boldsymbol{F}_{\mathrm{r}} \tag{7}$$

$$\boldsymbol{I}_{\mathrm{p}}\dot{\boldsymbol{\omega}}_{\mathrm{p}} = -\boldsymbol{\omega}_{\mathrm{p}}^{\times}\boldsymbol{I}_{\mathrm{p}}\boldsymbol{\omega}_{\mathrm{p}} + \boldsymbol{M}_{\mathrm{p}}^{\mathrm{aero}} + \boldsymbol{M}^{\mathrm{app}} - \boldsymbol{T}_{\mathrm{p-c}}\boldsymbol{T}_{\mathrm{b-c}}^{\mathrm{T}}\boldsymbol{M}_{\mathrm{r}} + \boldsymbol{X}_{\mathrm{cp}}^{\times}\boldsymbol{T}_{\mathrm{p-c}}\boldsymbol{F}_{\mathrm{r}} \tag{8}$$

where $\boldsymbol{z}_p = [-\sin\theta_{\mathrm{p}} \quad \sin\phi_{\mathrm{p}}\cos\theta_{\mathrm{p}} \quad \cos\phi_{\mathrm{p}}\cos\theta_{\mathrm{p}}]^{\mathrm{T}}$, $g \in \mathbb{R}$ is the gravity constant. $m_{\mathrm{p}} \in \mathbb{R}$ and the moment of inertia $\boldsymbol{I}_{\mathrm{p}} = \begin{bmatrix} I_{\mathrm{p}11} & 0 & I_{\mathrm{p}13} \\ 0 & I_{\mathrm{p}22} & 0 \\ I_{\mathrm{p}13} & 0 & I_{\mathrm{p}33} \end{bmatrix}$ are the mass of parafoil and the moment of inertia, respectively.

In particular, the aerodynamic forces and moments can be changed by the actual control input, i.e., asymmetrical flap deflection $\delta \in \mathbb{R}$. Denoting the span length and chord length of the parafoil as $b \in \mathbb{R}$ and $c \in \mathbb{R}$, the aerodynamic forces and moments can be modeled as

$$\boldsymbol{F}_{\mathrm{p}}^{\mathrm{aero}} = QS_{\mathrm{ref}}\boldsymbol{T}_{\mathrm{p-w}}\left(\boldsymbol{C}_{\mathrm{p}}^{\mathrm{aero}} + \boldsymbol{g}_1\delta\right) \tag{9}$$

$$\boldsymbol{M}_{\mathrm{p}}^{\mathrm{aero}} = QS_{\mathrm{ref}}\left(\boldsymbol{f}_{\mathrm{p}}^{\mathrm{aero}} + \boldsymbol{g}_2\delta\right) \tag{10}$$

where $Q \in \mathbb{R}$ is the dynamic pressure. Matrix $\boldsymbol{T}_{\mathrm{p-w}} \in \mathbb{R}^{3\times3}$ and vector $\boldsymbol{C}_{\mathrm{p}}^{\mathrm{aero}}, \boldsymbol{f}_{\mathrm{p}}^{\mathrm{aero}} \in \mathbb{R}^3$, $\boldsymbol{g}_1, \boldsymbol{g}_2 \in \mathbb{R}^3$ can refer to [26].

3.2. Dynamic Equations of the Payload

In this subsection, a payload dynamic equation with time-varying inertia would be established. The forces and moments of this subsystem primarily are due to four sources, i.e., aerodynamics, gravity, suspension lines, and time-varying inertia. Denoting $\boldsymbol{F}_{\mathrm{b}}^{\mathrm{aero}} \in \mathbb{R}^3$

and $\boldsymbol{M}_{\mathrm{b}}^{\mathrm{aero}} \in \mathbb{R}^3$ as the forces and moments due to aerodynamics, the payload dynamic equations can be described as follows:

$$m_b \dot{\boldsymbol{V}}_{\mathrm{b}} = m_{\mathrm{b}} g \boldsymbol{z}_{\mathrm{b}} + \boldsymbol{F}_{\mathrm{b}}^{\mathrm{aero}} - \boldsymbol{T}_{\mathrm{b-c}} \boldsymbol{F}_{\mathrm{r}} \tag{11}$$

$$\boldsymbol{I}_{\mathrm{b}} \dot{\boldsymbol{\omega}}_{\mathrm{b}} = -\boldsymbol{\omega}_{\mathrm{b}}^{\times} \boldsymbol{I}_{\mathrm{b}} \boldsymbol{\omega}_{\mathrm{b}} + \boldsymbol{M}_{\mathrm{b}}^{\mathrm{aero}} + \boldsymbol{M}_{\mathrm{r}} + \boldsymbol{X}_{\mathrm{cb}}^{\times} \boldsymbol{T}_{\mathrm{b-c}} \boldsymbol{F}_{\mathrm{r}} - \dot{\boldsymbol{I}}_{\mathrm{b}} \boldsymbol{\omega}_{\mathrm{b}} \tag{12}$$

where $\boldsymbol{z}_{\mathrm{b}} = [-\sin\theta_{\mathrm{b}} \quad \sin\phi_{\mathrm{b}}\cos\theta_{\mathrm{b}} \quad \cos\phi_{\mathrm{b}}\cos\theta_{\mathrm{b}}]^{\mathrm{T}}$. $m_{\mathrm{b}} \in \mathbb{R}$ and $\boldsymbol{I}_{\mathrm{b}} \in \mathbb{R}^{3\times 3}$ are the mass of payload and the moment of inertia, respectively.

As the parafoil and the payload are constrained by the suspension lines, the mathematical constraints between the subsystems's velocities are as follows:

$$\boldsymbol{V}_{\mathrm{c}} = \boldsymbol{T}_{\mathrm{p-c}}^{\mathrm{T}} \boldsymbol{V}_{\mathrm{p}} - \boldsymbol{T}_{\mathrm{p-c}}^{\mathrm{T}} \boldsymbol{\omega}_{\mathrm{p}}^{\times} \boldsymbol{X}_{\mathrm{cp}} = \boldsymbol{T}_{\mathrm{b-c}}^{\mathrm{T}} \boldsymbol{V}_{\mathrm{b}} - \boldsymbol{T}_{\mathrm{b-c}}^{\mathrm{T}} \boldsymbol{\omega}_{\mathrm{b}}^{\times} \boldsymbol{X}_{\mathrm{cb}} \tag{13}$$

Defining state vector of a PRS as $\boldsymbol{x} = \left[\boldsymbol{\omega}_{\mathrm{b}}^{\mathrm{T}} \quad \boldsymbol{\omega}_{\mathrm{p}}^{\mathrm{T}} \quad \boldsymbol{V}_{\mathrm{c}}^{\mathrm{T}} \quad \boldsymbol{F}_{\mathrm{r}}{}^{\mathrm{T}}\right]^{\mathrm{T}}$, the 9-DOF dynamic model of a PRS can be described as

$$\dot{\boldsymbol{x}} = \left([\boldsymbol{A}_1 \quad \boldsymbol{A}_2 \quad \boldsymbol{A}_3 \quad \boldsymbol{A}_4]^{\mathrm{T}}\right)^{-1} \begin{bmatrix} \boldsymbol{B}_1 \\ \boldsymbol{B}_2 \\ \boldsymbol{B}_3 \\ \boldsymbol{B}_4 \end{bmatrix} \tag{14}$$

where the terms of the matrix are

$$\boldsymbol{A}_1 = \left[\boldsymbol{0}_{3\times 3} \quad \boldsymbol{I}_{\mathrm{p}} + \boldsymbol{I}_{\mathrm{f}} \quad \boldsymbol{0}_{3\times 3} \quad \boldsymbol{X}_{\mathrm{cp}}^{\times} \boldsymbol{T}_{\mathrm{p-c}}\right]^{\mathrm{T}} \tag{15}$$

$$\boldsymbol{A}_2 = \left[-m_{\mathrm{b}} \boldsymbol{X}_{\mathrm{cb}}^{\times} \quad \boldsymbol{0}_{3\times 3} \quad m_{\mathrm{b}} \boldsymbol{T}_{\mathrm{b-c}} \quad \boldsymbol{T}_{\mathrm{b-c}}\right]^{\mathrm{T}} \tag{16}$$

$$\boldsymbol{A}_3 = \left[\boldsymbol{0}_{3\times 3} \quad -(m_{\mathrm{p}} \boldsymbol{I}_3 + \boldsymbol{M}_f) \boldsymbol{X}_{\mathrm{cp}}^{\times} \quad (m_{\mathrm{p}} \boldsymbol{I}_3 + \boldsymbol{M}_{\mathrm{f}}) \boldsymbol{T}_{\mathrm{p-c}} \quad -\boldsymbol{T}_{\mathrm{p-c}}\right]^{\mathrm{T}} \tag{17}$$

$$\boldsymbol{A}_4 = \left[\boldsymbol{I}_{\mathrm{b}} \quad \boldsymbol{0}_{3\times 3} \quad \boldsymbol{0}_{3\times 3} \quad -\boldsymbol{X}_{\mathrm{cb}}^{\times} \boldsymbol{T}_{\mathrm{b-c}}\right]^{\mathrm{T}} \tag{18}$$

$$\boldsymbol{B}_1 = \boldsymbol{M}_{\mathrm{p}}^{\mathrm{aero}} - \boldsymbol{\omega}_{\mathrm{p}}^{\times} (\boldsymbol{I}_{\mathrm{p}} + \boldsymbol{I}_{\mathrm{f}}) \boldsymbol{\omega}_{\mathrm{p}} - \boldsymbol{T}_{\mathrm{p-c}} \boldsymbol{T}_{\mathrm{b-c}}^{\mathrm{T}} \boldsymbol{M}_{\mathrm{r}} \tag{19}$$

$$\boldsymbol{B}_2 = \boldsymbol{F}_{\mathrm{b}}^{\mathrm{aero}} + m_{\mathrm{b}} g \boldsymbol{z}_{\mathrm{b}} - m_{\mathrm{b}} \boldsymbol{\omega}_{\mathrm{b}}^{\times} \boldsymbol{\omega}_{\mathrm{b}}^{\times} \boldsymbol{X}_{\mathrm{cb}} \tag{20}$$

$$\boldsymbol{B}_3 = \boldsymbol{F}_{\mathrm{p}}^{\mathrm{aero}} - (m_{\mathrm{p}} \boldsymbol{I}_3 + \boldsymbol{M}_{\mathrm{f}}) \boldsymbol{\omega}_{\mathrm{p}}^{\times} \boldsymbol{\omega}_{\mathrm{p}}^{\times} \boldsymbol{X}_{\mathrm{cp}} + m_{\mathrm{p}} g \boldsymbol{z}_{\mathrm{p}} - \boldsymbol{\omega}_{\mathrm{p}}^{\times} \boldsymbol{M}_{\mathrm{f}} \left(\boldsymbol{T}_{\mathrm{p-c}} \boldsymbol{V}_{\mathrm{c}} + \boldsymbol{\omega}_{\mathrm{p}}^{\times} \boldsymbol{X}_{\mathrm{cp}}\right) \tag{21}$$

$$\boldsymbol{B}_4 = \boldsymbol{M}_{\mathrm{b}}^{\mathrm{aero}} + \boldsymbol{M}_{\mathrm{r}} - \boldsymbol{\omega}_{\mathrm{b}}^{\times} \boldsymbol{I}_{\mathrm{b}} \boldsymbol{\omega}_{\mathrm{b}} - \dot{\boldsymbol{I}}_{\mathrm{b}} \boldsymbol{\omega}_{\mathrm{b}} \tag{22}$$

3.3. Kinematics Equations of the PRS

The rotational kinematics of the subsystem is modeled as

$$\dot{\boldsymbol{\Theta}}_i = \boldsymbol{G}_i \boldsymbol{\omega}_i \tag{23}$$

Relating the translational velocity and position by rotational transformation, the translational kinematics can be established by [32]

$$\begin{bmatrix} \dot{X}_{\mathrm{e}} \\ \dot{Y}_{\mathrm{e}} \\ \dot{Z}_{\mathrm{e}} \end{bmatrix} = \begin{bmatrix} V_{\mathrm{a}} \cos\psi_{\mathrm{p}} \\ V_{\mathrm{a}} \sin\psi_{\mathrm{p}} \\ -V_z \end{bmatrix} \tag{24}$$

where $V_{\mathrm{a}}, V_z \in \mathbb{R}$ are the horizontal and vertical components of the airspeed velocity.

3.4. Model Simplification and Problem Formulation

Actually, the parafoil attitude system (14) to (22) with disturbances and uncertainties can be combined as

$$\dot{\boldsymbol{\omega}}_{\mathrm{p}} = Q S_{\mathrm{ref}} \boldsymbol{I}_{\mathrm{p}}^{-1} \boldsymbol{g}_2 \delta + \boldsymbol{\tau}_{\mathrm{d}} \tag{25}$$

where $\boldsymbol{\tau}_\mathrm{d} = [\tau_{\mathrm{d}1} \quad \tau_{\mathrm{d}2} \quad \tau_{\mathrm{d}3}]^\mathrm{T}$ means the composite disturbance torques, which can be rewritten as

$$\boldsymbol{\tau}_\mathrm{d} = \boldsymbol{I}_\mathrm{p}^{-1}\left(QS_\mathrm{p}^\mathrm{ref}\boldsymbol{f}_\mathrm{p}^\mathrm{aero} - \boldsymbol{\omega}_2^\times(\boldsymbol{I}_\mathrm{p} + \boldsymbol{I}_\mathrm{f})\boldsymbol{\omega}_2 - \boldsymbol{T}_{\mathrm{p-c}}\boldsymbol{T}_{\mathrm{b-c}}^\mathrm{T}\boldsymbol{M}_\mathrm{r} - \boldsymbol{X}_\mathrm{cp}^\times\boldsymbol{T}_{\mathrm{p-c}}\boldsymbol{F}_\mathrm{r} - \boldsymbol{I}_\mathrm{f}\dot{\boldsymbol{\omega}}_2\right) \tag{26}$$

Differentiating the rotation kinematics equation of parafoil (23) results in

$$\frac{d\dot{\boldsymbol{\Theta}}_\mathrm{p}}{dt} = \boldsymbol{G}_\mathrm{p}\dot{\boldsymbol{\omega}}_\mathrm{p} + \boldsymbol{\tau}_\mathrm{f} \tag{27}$$

where $\boldsymbol{\tau}_\mathrm{f} = [\tau_{\mathrm{f}1} \quad \tau_{\mathrm{f}2} \quad \tau_{\mathrm{f}3}]^\mathrm{T} = \dot{\boldsymbol{G}}_\mathrm{p}\boldsymbol{\omega}_\mathrm{p}$ represents the available function in the system.

Using (25), (26), and (27), the dynamic model of parafoil can be obtained as

$$\frac{d\dot{\psi}_\mathrm{p}}{dt} = \frac{\sin\phi_\mathrm{p}}{\cos\theta_\mathrm{p}}\dot{\omega}_{\mathrm{p}2} + \frac{\cos\phi_\mathrm{p}}{\cos\theta_\mathrm{p}}\dot{\omega}_{\mathrm{p}3} + \tau_{\mathrm{f}3} \tag{28}$$

Defining $x_1 \triangleq \psi_\mathrm{p}$ and $x_2 \triangleq \dot{\psi}_\mathrm{p}$, the system (28) can be transformed into

$$\begin{cases} \dot{x}_1 = x_2 \\ \dot{x}_2 = \tau_{\mathrm{f}3} + g_\delta\delta + d \end{cases} \tag{29}$$

where $g_\delta = \frac{\cos\phi_\mathrm{p} b}{\cos\theta_\mathrm{p}\left(I_{\mathrm{p}13}^2 - I_{\mathrm{p}11}I_{\mathrm{p}33}\right)}\left(I_{\mathrm{p}13}C_{l\delta} - I_{\mathrm{p}33}C_{n\delta}\right)$ is the obtainable gain, and $d \in \mathbb{R}$ denotes the lumped disturbance caused by pitch angular velocity and other disturbances on yaw angular dynamics.

Assuming that a PRS has sufficient sensors and GPS to measure the parafoil attitude $\boldsymbol{\Theta}_\mathrm{p}$, system velocity V_a and position $\boldsymbol{X}_\mathrm{e}$, then the control objective is stated as follows. For a PRS described by (29), design a predefined-time heading controller to ensure that the desired path can be followed in a predefined time T_c despite uncertainties and the subsystem's coupling.

Remark 1. *Although there are some works introduced the 9-DOF model for describing the PRS, the proposed models cannot be directly used for control design. This work well in converting the high-fidelity model into an equivalent control model, providing a basis for the subsequent design of advanced control schemes.*

4. Development of Predefined-Time Heading Controller

In this section, an observer-based predefined-time control framework is proposed for a PRS to improve the convergence performance and following accuracy. As displayed in Figure 2, it consists of a predefined-time disturbance observer and a robust backstepping tracking controller combined with a predefined-time auxiliary system.

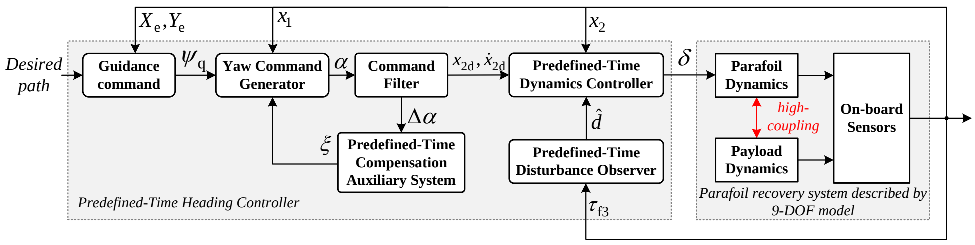

Figure 2. Diagram of the proposed observer-based predefined-time control framework.

4.1. *Predefined-Time Disturbance Observer*

The transformed system (29) can be rewritten into the linear-type form, such as

$$\dot{x}_2 = -x_2 + g_\delta\delta + \tau_\mathrm{lumped} \tag{30}$$

where the lumped disturbance torque is $\tau_{\text{lumped}} = x_2 + d + \tau_{\text{f3}}$.

A reference auxiliary system is defined as the similar dynamic form of (30)

$$\dot{x}_{\text{a}} = -x_{\text{a}} + g_{\delta}\delta \tag{31}$$

where $x_{\text{a}} \in \mathbb{R}$ is the state of the auxiliary system.

Denote the error between the state x_a and x_2 as $z = x_2 - x_a$. Then, differentiating z and inserting (30) and (31) leads to

$$\begin{cases} \dot{z} = \dot{x}_2 - \dot{x}_a = -z + \tau_{\text{lumped}} \\ y = z \end{cases} \tag{32}$$

where z is the state, and $y \in \mathbb{R}$ is denoted as the system's output.

On the basis of the preceding analysis, signal z is measurable. Define the estimated value of z as $\hat{z}$, and the observation error as $\tilde{z} = \hat{z} - z$. If the dynamic of $\hat{z}$ can be constructed, and the error $\tilde{z}$ is close to zero simultaneously, then the estimation $\hat{d}$ of d can be obtained. Hence, the following Theorem 1 can be given.

Theorem 1. *Design a predefined-time disturbance observer as*

$$\begin{cases} \dot{\hat{z}} = \dot{y} - \tilde{z} - \frac{\pi}{\eta T_{\text{c1}}}\left(0.5^{1-\frac{\eta}{2}}\text{sig}^{1-\eta}(\tilde{z}) + 0.5^{1+\frac{\eta}{2}}\text{sig}^{1+\eta}(\tilde{z})\right) \\ \hat{\tau}_{\text{lumped}} = \hat{d} - x_2 - \tau_{\text{f3}} \end{cases} \tag{33}$$

where $\hat{\tau}_{\text{lumped}} = \hat{z} + \dot{y}$, and $\dot{y}$ is the time derivative of y. $T_{\text{c1}} \in \mathbb{R}$ is the expected convergence time, $\eta \in (0,1)$ is a positive constant. Then, the observer error $\tilde{z}$ and the disturbance estimation error $\tilde{d} = \hat{d} - d$ show convergence to zero in a predefined time T_{c1}.

Proof of Theorem 1. Select the Lyapunov candidate as $V_1 = 0.5\tilde{z}^2$. It follows that

$$\begin{aligned} \dot{V}_1 &= \tilde{z}\dot{\tilde{z}} \\ &= \tilde{z}\left(\dot{y} - \tilde{z} - \frac{\pi}{\eta T_{c1}}\left(0.5^{1-\frac{\eta}{2}}\text{sig}^{1-\eta}(\tilde{z}) + 0.5^{1+\frac{\eta}{2}}\text{sig}^{1+\eta}(\tilde{z})\right) - \dot{z}\right) \\ &\leq -\frac{\pi}{\eta T_{c1}}\left(0.5^{1-\frac{\eta}{2}}|\tilde{z}|^{2-\eta} + 0.5^{1+\frac{\eta}{2}}|\tilde{z}|^{2+\eta}\right) \\ &= -\frac{\pi}{\eta T_{c1}}\left(V_1^{1-\frac{\eta}{2}} + V_1^{1+\frac{\eta}{2}}\right) \end{aligned} \tag{34}$$

Substituting (33) into (34) gives

$$\begin{aligned} \tilde{d} =& \hat{\tau}_{\text{lumped}} - x_2 - f - d \\ =& \hat{z} + \dot{y} - \tau_{\text{lumped}} \\ =& \tilde{z} \end{aligned} \tag{35}$$

According to Lemma 1, $\tilde{z} \equiv 0$ is achieved when $t \geq T_{\text{c1}}$, and thus $\tilde{d} \equiv 0$ is achieved when $t \geq T_{\text{c1}}$. It is proved that the total disturbance d could be estimated by $\hat{d}$ after a predefined time T_{c1}. □

Remark 2. *Although many finite-time or fixed-time disturbance observers have been designed at present, the literature on the study of predefined-time observers is still relatively limited. In addition, the design of this kind of observer often needs to know the upper bound of the lumped disturbance, and it is difficult to apply to an actual system with more external disturbances, such as the PRS. The observer proposed in this paper does not need to know the upper bound of the disturbance, which is convenient for control design.*

4.2. Predefined-Time Controller

Before designing the yaw angle controller, it is necessary to convert the heading error into the desired yaw angle signal $x_{1d} \in \mathbb{R}$. Denoting $[X_q \quad Y_q]^T \in \mathbb{R}^2$ and $\psi_q \in \mathbb{R}$ as the origin and the direction of the desired path, one obtains

$$\begin{cases} x_{1d} = -\psi^{\infty} \frac{2}{\pi} \arctan(k_1 y_e) \\ y_e = -\sin\psi_q (X_p - X_q) + \cos\psi_q (Y_p - Y_q) \end{cases} \tag{36}$$

where $k_1 \in \mathbb{R}_+$ is a positive constant which affects the transition rate from ψ^{∞} to zero. $y_e \in \mathbb{R}$ represents the straight path-following error. The orbit path-following error is constructed in a similar way of the straight path, as given in [33].

The backstepping control technique is then adopted to develop the predefined-time yaw controller for a PRS. According to the standard procedures of backstepping controller design, the time derivative of the desired yaw angular angle x_{2d} is necessitated; practically, it is difficult to obtain an accurate value through the numerical method. Hence, a differential state estimator α is introduced to solve the problem. Defining the yaw tracking error $e_1 = x_1 - \psi_q$, the variable α is designed as

$$\alpha = -0.5e_1 - \frac{\pi}{\eta T_{c2}} \left(0.5^{1-\frac{\eta}{2}} e_1^{1-\eta} + 0.5^{1+\frac{\eta}{2}} e_1^{1+\eta} \right) + \xi + \dot{\psi}_q \tag{37}$$

with a predefined-time compensation auxiliary system

$$\dot{\xi} = \begin{cases} -\xi - g_1\xi - \frac{\pi}{\eta T_{c2}} \left(0.5^{1-\frac{\eta}{2}} \mathrm{sig}^{1-\eta}(\xi) + 0.5^{1+\frac{\eta}{2}} \mathrm{sig}^{1+\eta}(\xi) \right) + \Delta\alpha & |\xi| > \varepsilon_{\xi} \\ 0 & |\xi| \leq \varepsilon_{\xi} \end{cases} \tag{38}$$

where $g_1 = \frac{|e_1\Delta\alpha| + 0.5\Delta\alpha^2}{\xi^2}$ represents a positive gain, and the $\Delta\alpha = x_{2d} - \alpha$ represents the estimation error.

Theorem 2. *For a RPS described by 9-DOF model, let the yaw tracking control law be designed as*

$$\delta = \frac{1}{g_{\delta}} \left(-e_1 - \hat{d} - \tau_{f3} - \frac{\pi}{\eta T_{c2}} \left(0.5^{1-\frac{\eta}{2}} e_2^{1-\eta} + 0.5^{1+\frac{\eta}{2}} e_2^{1+\eta} \right) + \dot{x}_{2d} \right) \tag{39}$$

where the angular angle tracking error $e_2 = x_2 - x_{2d}$. Then, the closed-loop system with estimator (37) and auxiliary system (38) can be stabilized with predefined-time convergence, even when subject to internal relative motions and aerodynamic uncertainties. Moreover, the yaw tracking error $e_1 \equiv 0$ is achieved when $t > T_c$, where T_c is a predefined time in advance.

Proof of Theorem 2. First of all, choose a Lyapunov candidate function as

$$V_2 = 0.5e_1^2 + 0.5\xi^2 \tag{40}$$

Substituting (38) into (40) results in

$$\begin{aligned} \dot{V}_2 =& e_1\dot{e}_1 + \xi\dot{\xi} \\ =& e_1(\alpha + \Delta\alpha + e_2 - \dot{\psi}_q) + \xi\dot{\xi} \\ =& e_1e_2 - \frac{\pi}{\eta T_{c2}} \left(0.5^{1-\frac{\eta}{2}} e_1^{2-\eta} + 0.5^{1+\frac{\eta}{2}} e_1^{2+\eta} \right) - 0.5e_1^2 + e_1\xi + e_1\Delta\alpha - \xi^2 \\ & - |e_1\Delta\alpha| - 0.5\Delta\alpha^2 - \frac{\pi}{\eta T_{c2}} \left(0.5^{1-\frac{\eta}{2}} \xi^{2-\eta} + 0.5^{1+\frac{\eta}{2}} \xi^{2+\eta} \right) + \xi\Delta\alpha \\ & \leq e_1e_2 - \frac{\pi}{\eta T_{c2}} \left(0.5^{1-\frac{\eta}{2}} e_1^{2-\eta} + 0.5^{1+\frac{\eta}{2}} e_1^{2+\eta} \right) - \frac{\pi}{\eta T_{c2}} \left(0.5^{1-\frac{\eta}{2}} \xi^{2-\eta} + 0.5^{1+\frac{\eta}{2}} \xi^{2+\eta} \right) \end{aligned} \tag{41}$$

Then, select another Lyapunov candidate function as $V_3 = 0.5e_2^2$; differentiating it and inserting (39) yields

$$\begin{aligned}\dot{V}_2 =& e_2(g_\delta \delta + \tau_{f3} + d - \dot{x}_{2d}) \\ =& e_2\left(-e_1 - \hat{d} - \tau_{f3} - \frac{\pi}{\eta T_{c2}}\left(0.5^{1-\frac{\eta}{2}} e_2^{1-\eta} + 0.5^{1+\frac{\eta}{2}} e_2^{1+\eta}\right) + \dot{x}_{2d} + \tau_{f3} + d - \dot{x}_{2d}\right) \\ =& e_2\left(-e_1 - \frac{\pi}{\eta T_{c2}}\left(0.5^{1-\frac{\eta}{2}} e_2^{1-\eta} + 0.5^{1+\frac{\eta}{2}} e_2^{1+\eta}\right) - \tilde{d}\right) \\ =& -e_1 e_2 - \frac{\pi}{\eta T_{c2}}\left(0.5^{1-\frac{\eta}{2}} e_2^{2-\eta} + 0.5^{1+\frac{\eta}{2}} e_2^{2+\eta}\right) - e_2 \tilde{d}\end{aligned} \tag{42}$$

According to Theorem 1, the observer error $\tilde{d} \equiv 0$ is achieved when $t \geq T_{c1}$. Hence, $\dot{V}_2 = -e_1 e_2 - \frac{\pi}{\eta T_{c2}}\left(0.5^{1-\frac{\eta}{2}} e_2^{2-\eta} + 0.5^{1+\frac{\eta}{2}} e_2^{2+\eta}\right)$ is achieved when $t \geq T_{c1}$.

To the end, choose a Lyapunov candidate function as $V = V_2 + V_3$, whose time derivative is given as

$$\begin{aligned}\dot{V} =& \dot{V}_2 + \dot{V}_3 \\ =& -\frac{\pi}{\eta T_{c2}}\left(0.5^{1-\frac{\eta}{2}} e_1^{2-\eta} + 0.5^{1+\frac{\eta}{2}} e_1^{2+\eta}\right) - \frac{\pi}{\eta T_{c2}}\left(0.5^{1-\frac{\eta}{2}} \xi^{2-\eta} + 0.5^{1+\frac{\eta}{2}} \xi^{2+\eta}\right) \\ & - \frac{\pi}{\eta T_{c2}}\left(0.5^{1-\frac{\eta}{2}} e_2^{2-\eta} + 0.5^{1+\frac{\eta}{2}} e_2^{2+\eta}\right) \\ \leq & -\frac{\pi}{\eta T_{c2}}\left(V^{1-\frac{\eta}{2}} + V^{1+\frac{\eta}{2}}\right)\end{aligned} \tag{43}$$

It is concluded that the closed-loop control system can be proved to be predefined time stable. The settling time of the yaw tracking error e_1 is T_c, i.e.,

$$T_c = \max\{T_{c1}, T_{c2}\} \tag{44}$$

which can be designed in advance. □

4.3. Convergence Analysis

Although the predefined-time stability of the yaw tracking system is proved above, the heading control system needs to be further analyzed. Substituting (24) in the time derivative of lateral error y_e gives

$$\begin{aligned}\dot{y}_e &= -\sin\psi_q \dot{X}_p + \cos\psi_q \dot{Y}_p \\ &= -\sin\psi_q V_a \cos\psi_p + \cos\psi_q V_a \sin\psi_p \\ &= V_a \sin(x_1 - \psi_q) \\ &= V_a \sin e_1\end{aligned} \tag{45}$$

It can be seen that the change rate of y_e will tend to be stable when $e_1 \equiv 0$. Substituting the controller (39) into the error dynamics yields

$$\begin{cases} \dot{e}_1 = -\frac{\pi}{\eta T_{c2}}\left(0.5^{1-\frac{\eta}{2}} \mathrm{sig}^{1-\eta}(e_1) + 0.5^{1+\frac{\eta}{2}} \mathrm{sig}^{1+\eta}(e_1)\right) \\ \dot{e}_2 = -e_1 - \tilde{d} - \frac{\pi}{\eta T_{c2}}\left(0.5^{1-\frac{\eta}{2}} e_2^{1-\eta} + 0.5^{1+\frac{\eta}{2}} e_2^{1+\eta}\right) \end{cases} \tag{46}$$

where $\tilde{d} = 0$ is achieved in Theorem 1 for $t > T_{c1}$.

To summarize, the heading tracking control system of a PRS described by 9-DOF is predefined time stable.

Remark 3. *According to Theorems 1 and 2, the time-derivative of y and x_{2d} are needed to implement the yaw tracking controller, which is difficult to obtain in practice. To solve the problem, fast high-*

order sliding-mode differentiators (FHOSMDs) are applied in this paper. The Kth FHOSMDs has the form of

$$\begin{cases} \dot{\zeta}_0 = v_0 = -\lambda_{0,1}(\zeta_0 - h) - \lambda_{0,2}\mathrm{sig}(\zeta_0 - h)^{k/(k+1)} + \zeta_1 \\ \dot{\zeta}_i = v_i = -\lambda_{i,1}(\zeta_i - v_{i-1}) - \lambda_{i,2}\mathrm{sig}(\zeta_i - v_{i-1})^{(k-i)/(k-i+1)} + \zeta_{i+1} \\ \vdots \\ i = 1, 2, \ldots, k-1 \\ \dot{\zeta}_n = v_n = -\lambda_{n,1}(\zeta_n - v_{n-1}) - \lambda_{n,2}\mathrm{sig}(\zeta_n - v_{n-1})^{7/9} \end{cases} \tag{47}$$

where $\lambda_{0,1}, \lambda_{0,2}, \ldots, \lambda_{n,2} \in \mathbb{R}^+$ are the positive gains, $\zeta_i \in \mathbb{R}$ is the state of the differentiators, and $i = 1, 2, \ldots, k-1$, $h \in \mathbb{R}$ is the input signal. When using the differentiators (47) to calculate $\dot{y}$ and $\dot{x}_{2\mathrm{d}}$, y and $x_{2\mathrm{d}}$ should be assigned to h, respectively.

Remark 4. *Compared with the finite-time controller or the fixed-time controller, the controller proposed in this paper is easier to set control parameters. The procedure of choosing control parameters is listed as follows: (a) set the desired convergence time T_c with the physical limitations and flight missions considered; (b) choose the gain $\eta \in (0,1)$ by trial and error. Generally, a smaller η is more appropriate.*

5. Results

In this section, numerical examples are carried out to verify the proposed controller. The parameters of the proposed heading tracking controller are chosen as $\eta = 0.3$, $T_{\mathrm{c}1} = 8$ s, and $T_{\mathrm{c}2} = 10$ s.

The parameters of the PRS described by the 9-DOF model are given in Table 1. Moreover, the moment of inertia about O_p is $\boldsymbol{I}_\mathrm{p} = \begin{bmatrix} 1356 & 0 & -84.24 \\ 0 & 1300 & 0 \\ -84.24 & 0 & 81.13 \end{bmatrix} \mathrm{kg} \cdot \mathrm{m}^2$, and the moment of inertia about O_b is $\boldsymbol{I}_\mathrm{b} = \begin{bmatrix} 421 & 0 & 0 \\ 0 & 421 & 0 \\ 0 & 0 & 421 \end{bmatrix} \mathrm{kg} \cdot \mathrm{m}^2$. The initial horizontal position of the PRS is $[0 \quad 100]$ m.

Table 1. Parameters of the parafoil and payload.

	Parameters	**Value**
Paraglider	Mass	20 kg
	Relative position	$[0 \quad 0 \quad -9.595]^\mathrm{T}$ m
	Span length	6.4 m
	Chord length	2.1 m
Payload	Mass	80 kg
	Relative position	$[0 \quad 0 \quad 2]^\mathrm{T}$ m
	Length	4 m
	Width	4 m
	Height	4 m

5.1. Predefined-Time Control Performance

In this subsection, the proposed predefined-time controller (denoted by PPTC) and the finite-time controller (denoted by FTC) [28] will conduct comparative simulation under different initial conditions. For fair comparison, a finite-time disturbance observer is designed to reconstruct and suppress the disturbance in the FTC. The resulted heading tracking errors of two controllers are illustrated in Figure 3. It is found that the PPTC achieves a faster converging rate than the FTC. More specifically, the convergence time of the PPTC is always less than the predefined time $T_\mathrm{c} = 10$ s, no matter what the initial value is. On the contrary, the convergence time of the FTC is affected by the initial value. According to Figure 4, the maximum required control powers for the two controllers are almost equivalent, implying the better performance of the PPTC.

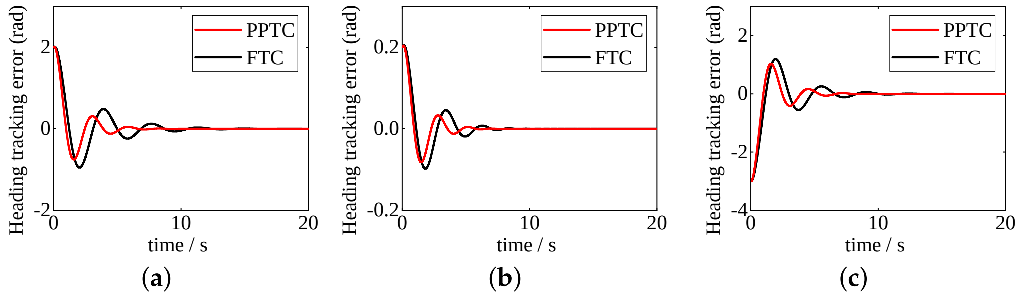

Figure 3. The heading tracking errors of the PPTC and FTC(**a**) Case 1; (**b**) Case 2; (**c**) Case 3.

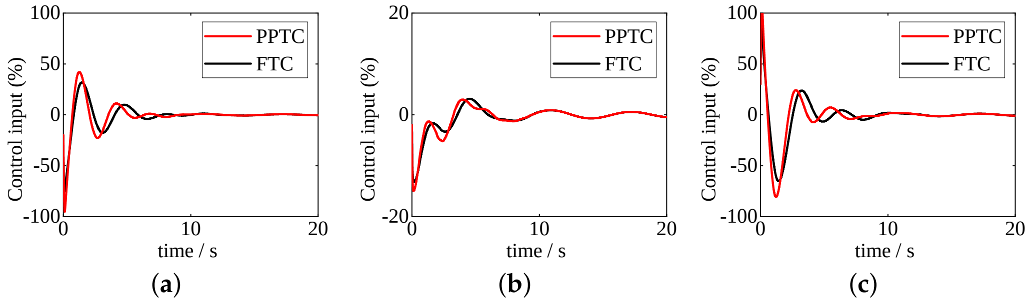

Figure 4. The control inputs of the PPTC and FTC. (**a**) Case 1; (**b**) Case 2; (**c**) Case 3.

5.2. Comparison with the Existing Heading Controller

In this subsection, the presented predefined-time heading tracking controller is applied to the PRS to follow the straight-line and orbit path. Suppose that the origin of the desired straight-line path is $[0 \quad 0]^T$ m and the direction is $\psi_q = 0.707$ rad; then, the simulation result is given in Figure 5. Define the origin of the desired orbit path as $[0 \quad 0]^T$ m and the desired radius as 100 m, then the simulation result is shown in Figure 6. Because other dynamics can gradually stabilize as long as an appropriate heading control method is adopted, this section only shows the main states of the PRS. Although that PPTC and PID controller successfully accomplish the following maneuvering, it can be seen that the PPTC provides smaller steady-state error than the PID controller for the PRS subject to internal relative motions and disturbances.

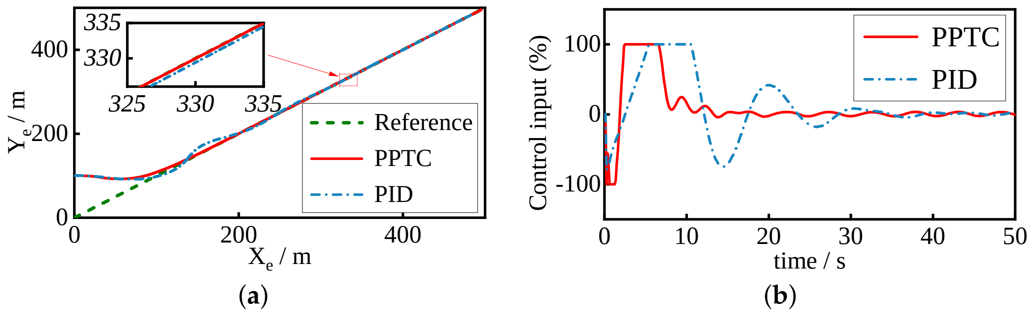

Figure 5. Heading tracking results for following straight-line path. (**a**) Straight -line tracking result; (**b**) control input for following straight-line path.

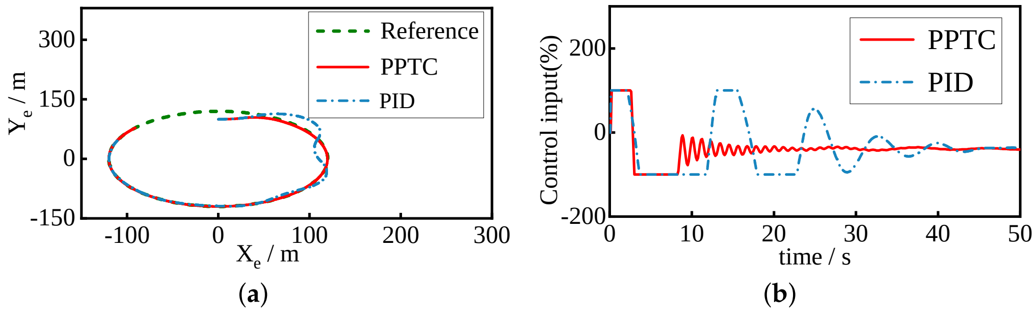

Figure 6. Heading tracking results for following orbit path. (**a**) Orbit tracking result; (**b**) control input for following orbit path.

5.3. Hardware-in-Loop Testing Results

To further validate the effectiveness of the proposed control law, a hardware-in-loop testing platform is used, shown in Figure 7. The hardware-in-loop testing platform consists of a simulation model of PRS, an airborne controller, and a canopy. The airborne controller is composed of an STM32F103 device, and two actuators with potentiometers. Additionally, a 4200 mA·h battery provides power for the airborne controller. It is noteworthy that the simulation model and the STM32 use the user datagram protocol (UDP) for data transmission. The status information of the PRS is transferred from the model computer to the STM32. According to the status information, STM32 uses the proposed method to generate the corresponding control signal. Then, the control signal is converted into pulse width modulation (PWM) and transmitted to actuators to pull the control ropes. After that, the potentiometers transmit the angle change back to the STM32 as a voltage and convert it into a digital signal to the computer. This process is a more realistic scenario.

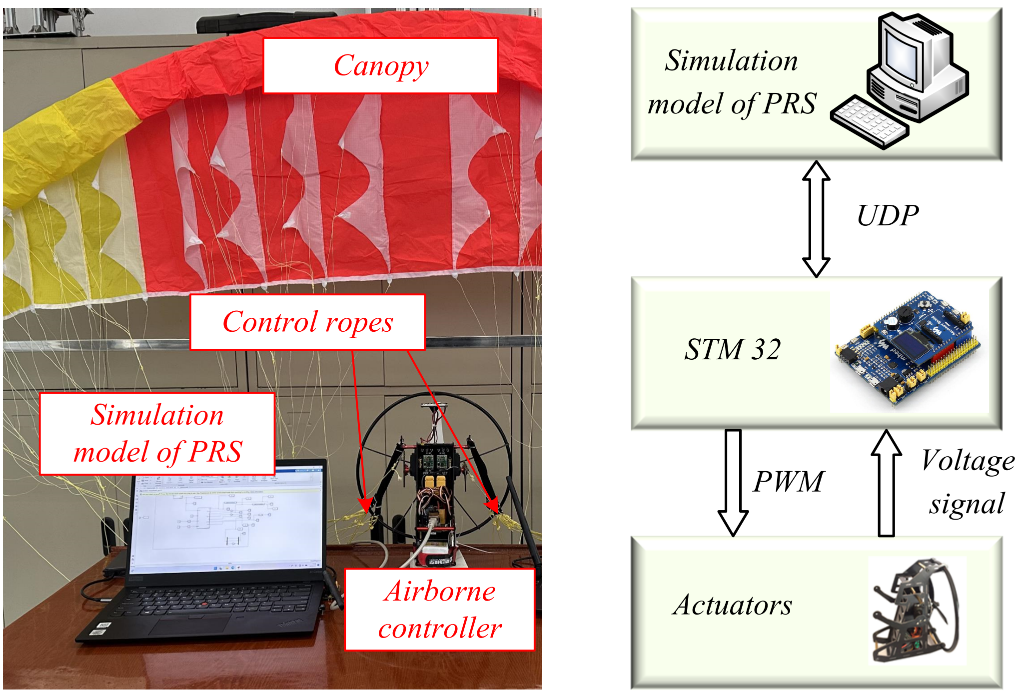

Figure 7. System configuration of hardware-in-loop test.

In order to simulate a more real situation, white noise is used to simulate sensor error before the state output. Based on this testing platform, the testing results for the case of following the straight-line path are given in Figure 8.

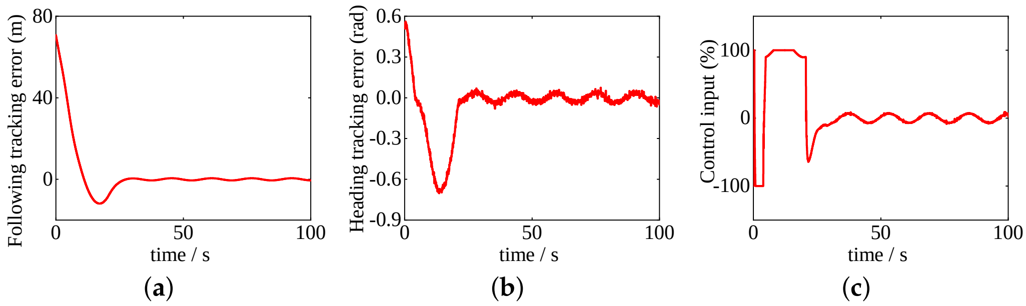

Figure 8. Hardware-in-loop testing results. (**a**) Following tracking error; (**b**) heading tracking error; (**c**) control input.

As given in Figure 8, even with the disturbances of hardware delay and measurement noise, the proposed controller can make the heading tracking system stable. In this experiment, the dynamic effect of tracking is not as stable as the simulation result because of the delay of the actuators. Despite this, it is seen that the proposed method can be utilized for this hardware-in-loop testing platform, which implies that this method has the basis for practical parafoil systems.

6. Conclusions

Although there are lots of investigations on designing heading control for the PRS, few of them address the predefined-time control problem with internal relative motions and external apparent mass considered simultaneously. To handle the problem, this paper proposed an observer-based predefined-time controller for the 9-DOF model of a PRS. The closed-loop heading control system is guaranteed to be predefined time stable. The simulation results show that the proposed controller has better control performance than FTC and PID controllers. The proposed heading control method can be applied to other vehicles, such as unmanned vehicles, autonomous ships, and so on. Future work will develop the heading control problem considering the PRS constraints explicitly, and verify the proposed method on the flight testing platform.

Author Contributions: Conceptualization, Y.G. and J.Y.; methodology, Y.G. and X.X.; software, Y.G.; validation, Y.G., X.W. and L.L.; writing—original draft preparation, Y.G.; supervision, J.Y. and X.X. All authors have read and agreed to the published version of the manuscript.

Funding: This research has been funded by the National Natural Science Foundation of China (No. 62273283) and Industry-University-Research Innovation Fund in Ministry of Education of China (No. 2021ZYA03006).

Data Availability Statement: Not applicable.

Conflicts of Interest: The authors declare no conflict of interest.

Sample Availability: The datasets generated during and/or analyzed during the current study are available from the corresponding author on reasonable request.

Abbreviations

The following abbreviations are used in this manuscript:

PRS	Parafoil recovery system
DOF	Degrees-of-freedom
PID	Proportional-integral-differential
PPTC	Proposed predefined-time controller
FTC	Finite-time controller

References

1. Rimani, J.; Viola, N.; Saluzzi, A. An Approach to the Preliminary Sizing and Performance Assessment of Spaceplanes' Landing Parafoils. *Aerospace* **2022**, *9*, 823. [CrossRef]
2. Dek, C.; Overkamp, J.L.; Toeter, A.; THoppenbrouwer, o.; Slimmens, J.; van Zijl, J.; Rossi, P.A.; Machado, R.; Hereijgers, S.; Kilic, V.; et al. A recovery system for the key components of the first stage of a heavy launch vehicle. *Aerosp. Sci. Technol.* **2020**, *100*, 105778. [CrossRef]
3. Sun, H.; Sun, Q.; Zeng, X.; Luo, S.; Wu, W.; Chen, Z. Accurate homing of parafoil delivery systems based glide-ratio control. *IEEE Trans. Aerosp. Electron. Syst.* **2019**, *56*, 2374–2389. [CrossRef]
4. Tanaka, K.; Tanaka, M.; Iwase, A.; Wang, H.O. A rational polynomial tracking control approach to a common system representation for unmanned aerial vehicles. *IEEE/ASME Trans. Mechatronics* **2020**, *25*, 919–930. [CrossRef]
5. Tanaka, M.; Tanaka, K.; Wang, H.O. Practical model construction and stable control of an unmanned aerial vehicle with a parafoil-type wing. *IEEE Trans. Syst. Man, Cybern. Syst.* **2017**, *49*, 1291–1297. [CrossRef]
6. Cacan, M.R.; Scheuermann, E.; Ward, M.; Costello, M.; Slegers, N. Autonomous airdrop systems employing ground wind measurements for improved landing accuracy. *IEEE/ASME Trans. Mechatronics* **2015**, *20*, 3060–3070. [CrossRef]
7. Zhang, S.Y.; Yu, L.; Wu, Z.H.; Jia, H.; Liu, X. Numerical investigation of ram-air parachutes inflation with fluid-structure interaction method in wind environments. *Aerosp. Sci. Technol.* **2021**, *109*, 106400. [CrossRef]
8. Slegers, N.; Costello, M. Aspects of control for a parafoil and payload system. *J. Guid. Control. Dyn.* **2003**, *26*, 898–905. [CrossRef]
9. Guo, Y.; Yan, J.; Wu, C.; Wu, X.; Xiao, B. Adaptive vector field-based accurate homing control of aerial delivery systems. *Chin. J. Aeronaut.* **2022**, *36*, 256–269. [CrossRef]
10. Wu, W.; Sun, Q.; Sun, M.; Dehmer, M.; Chen, Z. Modeling and control of parafoils based on computational fluid dynamics. *Appl. Math. Model.* **2019**, *70*, 378–401. [CrossRef]
11. Strickert, G. Study on the relative motion of parafoil-load-systems. *Aerosp. Sci. Technol.* **2004**, *8*, 479–488. [CrossRef]
12. Zhang, Z.; Zhao, Z.; Fu, Y. Dynamics analysis and simulation of six DOF parafoil system. *Clust. Comput.* **2019**, *22*, 12669–12680. [CrossRef]
13. Slegers, N.; Gorman, C. Comparison and analysis of multi-body parafoil models with varying degrees of freedom. In Proceedings of the AIAA aerodynamic Decelerator Systems Technology Conference and Seminar, Seattle, WA, USA, 4–7 May 2011; p. 2615.
14. Slegers, N. Comparison of parafoil dynamic modes with varying payload connections. In Proceedings of the AIAA Aerodynamic Decelerator Systems Technology Conference, Denver, CO, USA, 5–9 June 2017; p. 3878.
15. Zhu, E.; Sun, Q.; Tan, P.; Chen, Z.; Kang, X.; He, Y.-P. Modeling of powered parafoil based on Kirchhoff motion equation. *Nonlinear Dyn.* **2015**, *79*, 617–629. [CrossRef]
16. Tan, P.; Sun, M.; Sun, Q.; Chen, Z. Dynamic modeling and experimental verification of powered parafoil with two suspending points. *IEEE Access* **2020**, *8*, 12955–12966. [CrossRef]
17. Prakash, O.; Daftary, A.; Ananthkrishnan, N. Trim and stability analysis of parafoil/payload system using bifurcation methods. In Proceedings of the AIAA Aerodynamic Decelerator Systems Technology Conference and Seminar, Munich, Germany, 23–26 May 2005; p. 1666.
18. Slegers, N.; Costello, M. Model predictive control of a parafoil and payload system. *J. Guid. Control. Dyn.* **2005**, *28*, 816–821. [CrossRef]
19. Chiel, B.S. Adaptive control of a 10K parafoil system. In Proceedings of the AIAA Aerodynamic Decelerator Systems Technology Conference, Daytona Beach, FL, USA, 30 March–2 April 2015; p. 2107.
20. Rademacher, B.; Lu, P.; Strahan, A.; Cerimele, C. Trajectory design, guidance and control for autonomous parafoils. In Proceedings of the AIAA Guidance, Navigation and Control Conference and Exhibit, Honolulu, HI, USA, 18–21 August 2008; p. 7417.
21. Lee, S.J.; Arena, A. Autonomous parafoil return-to-point vehicle for high altitude ballooning. In Proceedings of the AIAA Guidance, Navigation, and Control Conference, Portland, OR, USA, 8–11 August 2014; p. 0974.
22. Ward, M.; Costello, M. Adaptive glide slope control for parafoil and payload aircraft. *J. Guid. Control. Dyn.* **2013**, *36*, 1019–1034. [CrossRef]
23. Omar, H.M. Optimal Geno-Fuzzy Lateral Control of Powered Parachute Flying Vehicles. *Aerospace* **2021**, *8*, 400. [CrossRef]
24. Prakash, O. NDI bases Generic Heading Tracking Control Law for Parafoil/payload System. In Proceedings of the AIAA Aviation 2020 Forum, Virtual, 15–19 June 2020; p. 3195.
25. Luo, S.; Sun, Q.; Tan, P.; Sun, M.; Chen, Z.; He, Y. Soft landing control of unmanned powered parafoils in unknown wind environments. *Proc. Inst. Mech. Eng. Part G J. Aerosp. Eng.* **2019**, *233*, 949–968. [CrossRef]
26. Guo, Y.; Yan, J.; Wu, C.; Xiao, B. Modeling and practical fixed-time attitude tracking control of a paraglider recovery system. *ISA Trans.* **2022**, *128*, 391–401. [CrossRef]
27. Tao, J.; Sun, Q.; Tan, P.; Chen, Z.; He, Y. Active disturbance rejection control (ADRC)-based autonomous homing control of powered parafoils. *Nonlinear Dyn.* **2016**, *86*, 1461–1476. [CrossRef]
28. Guo, Y.; Yan, J.; Xing, X.; Li, L.; Wu, C.; Wu, X. Finite-Time Disturbance Observer-Based Tracking Control for a Powered Parafoil System. In *Advances in Guidance, Navigation and Control, Proceedings of the 2022 International Conference on Guidance, Navigation and Control, Harbin, China, 5–7 August 2023;* Springer: Singapore, 2023. [CrossRef]
29. Wu, C.; Yan, J.; Qian, X.; Guo, Y.; Qu, Y. Predefined-time attitude stabilization of receiver aircraft in aerial refueling. *IEEE Trans. Circuits Syst. II Express Briefs* **2021**, *68*, 3321–3325. [CrossRef]

30. Sánchez-Torres, J.D.; Muñoz-Vázquez, A.J.; Defoort, M.; Aldana-López, R.; Gómez-Gutiérrez, D. Predefined-time integral sliding mode control of second-order systems. *Int. J. Syst. Sci.* **2020**, *51*, 3425–3435. [CrossRef]
31. Munoz-Vazquez, A.J.; Sánchez-Torres, J.D.; Jimenez-Rodriguez, E.; Loukianov, A.G. Predefined-time robust stabilization of robotic manipulators. *IEEE/ASME Trans. Mechatronics* **2019**, *24*, 1033–1040. [CrossRef]
32. Guo, Y.; Yan, J.; Wu, C.; Wu, X.; Chen, M.; Xing, X. Autonomous homing design and following for parafoil/rocket system with high-altitude. *J. Intell. Robot. Syst.* **2021**, *101*, 1–15. [CrossRef]
33. Nelson, D.R.; Barber, D.B.; McLain, T.W.; Beard, R.W. Vector field path following for miniature air vehicles. *IEEE Trans. Robot.* **2007**, *23*, 519–529. [CrossRef]